State-of-Charge Estimation of Lithium-Ion Battery Using Square Root Spherical Unscented Kalman Filter (Sqrt-UKFST) in Nanosatellite

Htet Aung, *Student Member, IEEE*, Kay Soon Low, *Senior Member, IEEE*, and Shu Ting Goh

Abstract—State-of-charge (SOC) estimation is an important aspect for modern battery management system. Dynamic and closed loop model-based methods such as extended Kalman filter (EKF) have been extensively used in SOC estimation. However, the EKF suffers from drawbacks such as Jacobian matrix derivation and linearization accuracy. In this paper, a new SOC estimation method based on square root unscented Kalman filter using spherical transform (Sqrt-UKFST) with unit hyper sphere is proposed. The Sqrt-UKFST does not require the linearization for nonlinear model and uses fewer sigma points with spherical transform, which reduces the computational requirement of traditional unscented transform. The square root characteristics improve the numerical properties of state covariance. The proposed method has been experimentally validated. The results are compared with existing SOC estimation methods such as Coulomb counting, portable fuel gauge, and EKF. The proposed method has an absolute root mean square error (RMSE) of 1.42% and an absolute maximum error of 4.96%. These errors are lower than the other three methods. When compared with EKF, it represents 37% and 44% improvement in RMSE and maximum error respectively. Furthermore, the Sqrt-UKFST is less sensitive to parameter variation than EKF and it requires 32% less computational requirement than the regular UKF.

Index Terms—Lithium-ion batteries, spherical unscented transform, square root unscented Kalman filter, state-of-charge (SOC).

I. INTRODUCTION

LITHIUM-ION battery has gained its popularity as the energy source for many applications ranging from portable equipment, electric vehicles, renewable energy systems to satellite application. The lithium-ion battery has higher energy densities, low self-discharge rate, and long cycle life when compared to other battery types such as lead acid and nickel cadmium [1]. However, over-charging and discharging of lithium-ion battery can cause an irreversible damage to the battery which compromises its performance and life span. To safeguard the safety and performance of the battery, a reliable and accurate state-of-charge (SOC) estimation method is highly desired in modern battery management system [2].

Several SOC estimation methods have been presented in the literatures [3]–[14]. Among them, the Coulomb counting

method is the most popular due to its simplicity and low computational cost. However, its accuracy depends on the sensor accuracy. Its performance also suffers from the initial error and the accumulated measurement errors. The Coulomb counting method is an open loop estimator as it only relies on the integration of current flowing in and out of the battery. The accumulated current measurement errors can give erroneous estimation as high as 25%.

An improved Coulomb counting method which uses the charging/discharging cut off voltage for periodic reset has been presented in [15], [16]. However, the voltage is highly dependent on the current magnitude, and a fully charging/discharging cycle is required. In [10], the SOC is estimated from the electromotive voltage (EMF) estimation using the impedance and load current. As it requires the alternative current (AC) to measure the impedance, it is more suitable for laboratory test but not in the actual application.

Computational intelligence methods using fuzzy logic and artificial neural networks [12], [17] have been developed for SOC estimation. Although it provides an accurate estimation, its computational cost is high. In addition, it suffers from the training process and the quality of training data set. Recently, the impulse response (IR) method [8] and the multivariate adaptive regression splines (MARS) technique [4] have been implemented for the SOC estimation. The IR method requires a pre-stored look up table to determine the SOC, and the MARS technique's accuracy has a limited operating range (25–90% of the SOC).

The state space based SOC and state of health (SOH) estimation method such as the H_∞ observer [18], the sliding mode observer [6], [19], [20], and the extended Kalman filter (EKF) [5], [7], [9], [21] have been reported in the literatures. Although sliding mode observer can handle the nonlinearity effects of the model well, its performance deteriorates when there is noise in the output. The EKF has been widely used for the SOC estimation. However, the linearized approximations of nonlinear function (or Jacobian matrix) in EKF increases the implementation complexity. In addition, its error convergence is sensitive to the initial state estimation error, and inaccurate Jacobian matrix estimation could lead to filter divergence and affect its stability.

To overcome these shortcomings, the square root unscented Kalman filter with spherical transform (Sqrt-UKFST) in a unit hyper sphere is proposed for the SOC estimation in this paper. The Sqrt-UKFST does not require the linearization for a nonlinear model, and it has a higher error order (second order) than EKF (first order) [22]. In addition, the Sqrt-UKFST does not
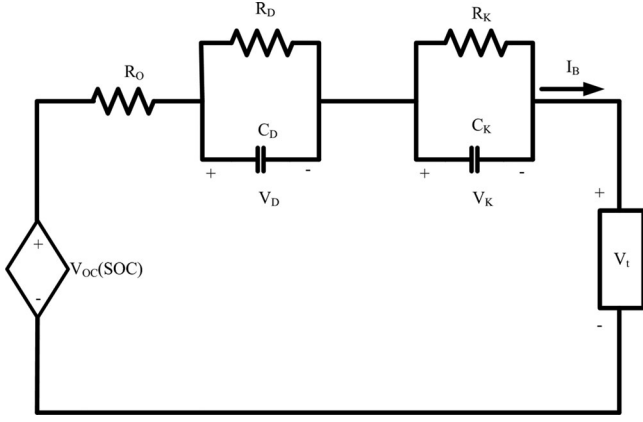
Fig. 1. Equivalent circuit model of lithium-ion battery.

Fig. 2. V_{OC} versus SOC graph.

require refactorization on state covariance as in the regular unscented Kalman filter (UKF). The spherical transform requires fewer sigma points than the regular UKF leading to lower computational cost [23]–[26]. Furthermore, the spherical transform requires only one weighting parameter instead of three required by the regular UKF. To allow a better controllability of sigma point distribution, a unit hyper sphere model is introduced in this paper such that the distribution is independent of the number of sigma points as in the standard spherical transform method.
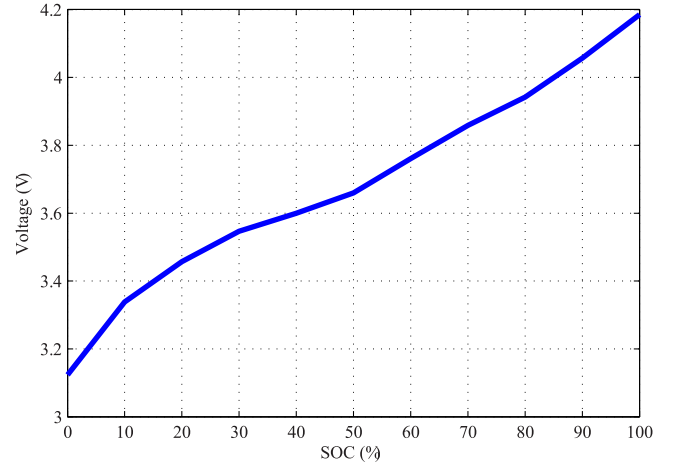
The proposed method has been validated with experimental results and benchmarked with EKF, a portable fuel gauge integrated circuit and the Coulomb counting methods. The results have shown that the proposed Sqrt-UKFST has a lower absolute mean, absolute maximum and root mean square error (RMSE) than all the other methods. Furthermore, it is computationally more efficient than regular UKF.

The outline of this paper is as follows. In Section II, the lithium-ion battery model and the battery parameters extraction are presented. Section III presents the proposed Sqrt-UKFST SOC estimation approach. Section IV shows the experimental setup and results. Section V concludes this paper.

II. LITHIUM-ION BATTERY MODEL

Different battery models have been proposed to describe the battery operations in the literature. It can be divided into two broad categories namely the electrochemical and equivalent circuit models [27]. Electrochemical model uses electrochemical laws to describe the battery operations. However, this method is computationally intensive and is more suitable for the study of electrode and electrolyte aspects. Equivalent circuit model uses electrical components such as resistors and capacitors to model the battery dynamic operations [28], [29]. It is simpler than the electrochemical models and is able to capture the battery dynamic response accurately. Thus, it is more suitable for control and simulation purposes.

Fig. 1 shows the double polarization model of a lithium-ion battery [30], [31]. The resistor R_O represents the instantaneous voltage drop during the battery charge/discharge process. Two resistor–capacitor (RC) networks are used to model the relax-

ation effects of battery charge/discharge process. In general, it provides a better modeling accuracy than a single RC network battery model [32]. The R_D and C_D network branch models the short term transient response of battery, whereas R_K and C_K are used to represent the long term transient response. In the circuit, the V_{OC} represents the battery open circuit voltage (OCV), V_t is the battery terminal voltage and I_B is the battery current.

A. Relationship Between Open Circuit Voltage and State of Charge

The OCV of the battery V_{OC} has a nonlinear relationship with SOC. To obtain this nonlinear function, the OCV test is conducted using the Panasonic NCR 18650 lithium battery with 2.9 Ah capacity as a case study. In this study, the hysteresis effect is neglected. The hysteresis effect can be included if an additional voltage source is placed in parallel to V_{oc} in Fig. 1 at the expense of increased complexity. The battery is first fully charged through the CC–CV method and is then rested for an hour to allow it to reach the steady state voltage before V_{OC} is measured. For the subsequent V_{OC} measured at different SOC levels, the battery is discharged at 0.29 A for an hour, and rested for another hour to reach the steady state before another test is conducted. Fig. 2 shows the SOC − V_{OC} graph obtained from the experiment.

To describe the relationship between the OCV and the SOC in Fig. 2, a polynomial curve fitting is used

$$V_{\mathrm{OC}} = f(\zeta) = m_1 \zeta^7 + m_2 \zeta^6 + \cdots + m_6 \zeta^2 + m_7 \zeta + m_8 \tag{1}$$

where ζ denotes the SOC. Based on the experimental data in Fig. 2, the coefficients are obtained as: $m_1 = -20.553$, $m_2 = 80.694$, $m_3 = -120.81$, $m_4 = 83.352$, $m_5 = -22.502$, $m_6 = -1.542$, $m_7 = 2.418$, and $m_8 = 3.124$. A seventh-order equation is found to be adequate yielding an error norm of 0.0195. This V_{OC} and ζ relationship is used in the estimation of battery terminal voltage in the next section.

B. Battery State Space Equations

Denote the SOC of the battery as ζ, and it can be expressed in discrete time as

$$\zeta_{k+1} = \zeta_k - \frac{\eta I_B \Delta t}{Q_b} \qquad (2)$$

where Q_b is the battery discharge capacity, I_B is the battery current, Δt is the sampling time, and η is the Coulomb efficiency. Using Kirchhoff's circuit laws, the circuit dynamics of the two RC networks can be written as

$$\dot{V_D} = -\frac{V_D}{R_D C_D} + \frac{I_B}{C_D} \qquad (3)$$

$$\dot{V_K} = -\frac{V_K}{R_K C_K} + \frac{I_B}{C_K}. \qquad (4)$$

Taking $\begin{bmatrix} \zeta & V_D & V_K \end{bmatrix}^T$ as the state variables, the battery state space equation can be described using (2)–(4) as

$$
\begin{bmatrix} \zeta_{k+1} \\ V_{D_{k+1}} \\ V_{K_{k+1}} \end{bmatrix} = F(\zeta, V_D, V_K) = \begin{bmatrix} 1 & 0 & 0 \\ 0 & e^{-\frac{\Delta t}{R_D C_D}} & 0 \\ 0 & 0 & e^{-\frac{\Delta t}{R_K C_K}} \end{bmatrix}
$$

$$
\times \begin{bmatrix} \zeta_k \\ V_{D_k} \\ V_{K_k} \end{bmatrix} + \begin{bmatrix} -\frac{\Delta t}{Q_b} \\ R_D(1 - e^{-\frac{\Delta t}{R_D C_D}}) \\ R_K(1 - e^{-\frac{\Delta t}{R_K C_K}}) \end{bmatrix} [I_B]. \quad (5)
$$

From Fig. 1, taking the battery terminal voltage, V_t, as the system output and the battery current, I_B, as the system input, the V_t measurement function H can be obtained as

$$
V_t = H(f(\zeta), V_D, V_K) = \begin{bmatrix} 1 & -1 & -1 \end{bmatrix} \begin{bmatrix} f(\zeta) \\ V_D \\ V_K \end{bmatrix} - I_B R_O. \quad (6)
$$

To estimate ζ, V_D, and V_K, the battery parameters (R_O, R_D, R_K, C_D, and C_K) are required. These parameters will be experimentally identified and discussed in the next section.

C. Battery Parameters Extraction

In this study, the transfer function method is used to identify the required battery parameters. Using (3)–(4), the battery terminal voltage in the frequency domain can be written as

$$V_t(s) = V_{OC}(s) - I_B(s)R_O - \frac{R_D I_B(s)}{1 + R_D C_D s} - \frac{R_K I_B(s)}{1 + R_K C_K s}. \quad (7)$$

By considering $V_t - V_{OC}$ as the output and the current I_B as the input, the transfer function $G(s)$ can be derived as

$$G(s) = \frac{V_t(s) - V_{OC}(s)}{I_B(s)} = -\frac{a_2 s^2 + a_1 s + a_0}{s^2 + b_1 s + b_0}$$

$$= -\left\{ \frac{R_O s^2 + \left(\frac{R_O}{R_D C_D} + \frac{R_O}{R_K C_K} + \frac{1}{C_D} + \frac{1}{C_K}\right) s + \frac{R_O + R_D + R_K}{R_D C_D R_K C_K}}{s^2 + \left(\frac{1}{R_D C_D} + \frac{1}{R_K C_K}\right) s + \frac{1}{R_D C_D R_K C_K}} \right\}. \quad (8)$$
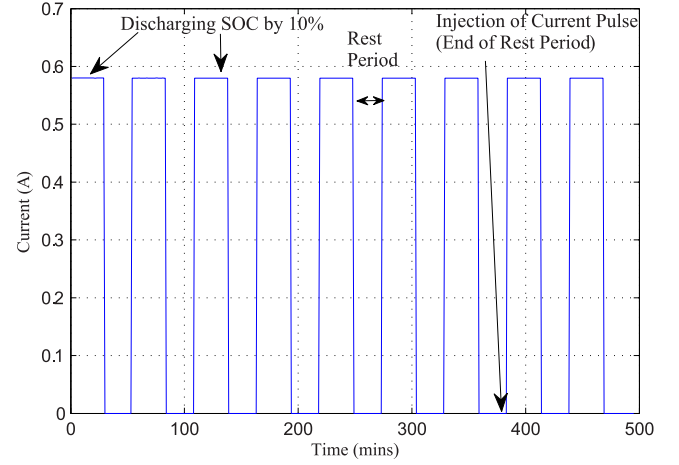

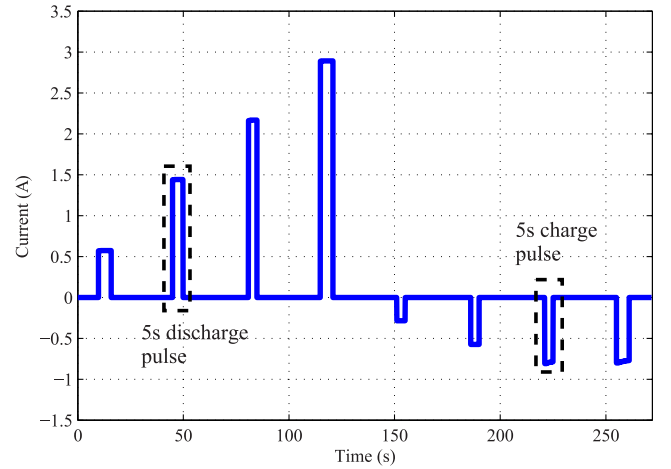Fig. 3. Battery parameters extraction discharge current profile.

Fig. 4. Injected discharge pulses at the end of each rest period.

To extract the battery parameters, various charge/discharge pulses are injected into the battery at different SOC intervals and the corresponding voltage responses are measured. To obtain the required voltage responses, the battery is fully charged through the CC–CV method. It is then discharged at 0.58 A for 30 min with 30 min rest interval as shown in Fig. 3. At the end of each rest interval, different charge (0.29, 0.58, 1.16, and 1.45 A) and discharge (0.58, 1.45, 2.175, and 2.9 A) current pulses with 5 s duration are injected into the battery, as shown in Fig. 4. Assuming V_{OC} remains unchanged over the short duration, the corresponding voltage responses with respect to each current pulse are recorded. The cycle is repeated at every 10% SOC interval until the battery is fully discharged. The voltage responses from the injected current pulses across different SOC are then used in identifying the transfer function and the parameter identification. Fig. 5 shows one example of the voltage responses at 90% SOC.

Using the voltage responses and the corresponding injected current pulses, the transfer function coefficients (a_2, a_1, a_0, b_1, and b_0) of $G(s)$ can be obtained. The battery parameters (R_O,
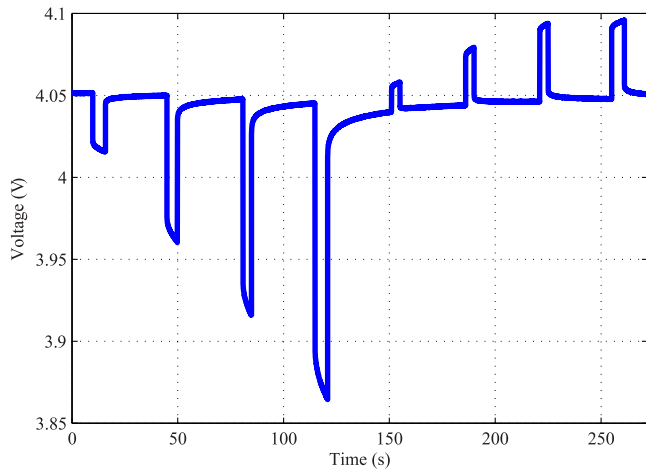
Fig. 5.   Discharge pulses voltage responses at 90% SOC.

TABLE I
IDENTIFIED BATTERY PARAMETERS

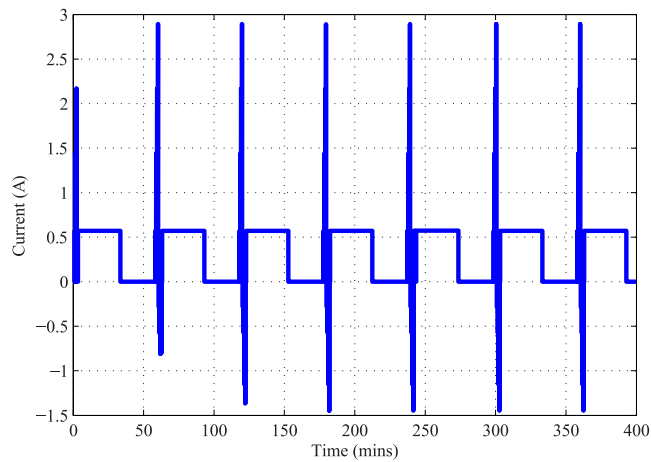|	
R_O	54.28 mΩ
R_D	10.58 mΩ
R_K	40.16 mΩ
C_D	330 F
C_K	1020 F

Fig. 6.   HPPC load profile.

R_D, C_D, R_K, and C_K) can then be obtained by solving these coefficients. Different set of transfer functions and parameters are identified with respect to each measure voltage at each SOC level. As the variation of parameters with respect to SOC are insignificant, the average identified parameters are used. Table I lists the identified battery parameters.

To verify the identified battery parameters, a hybrid pulse power characterization (HPPC) load profile as shown in Fig. 6 is used [9]. The comparison of experimental and estimated voltages as well as the estimation error are shown in Figs. 7 and 8 respectively.
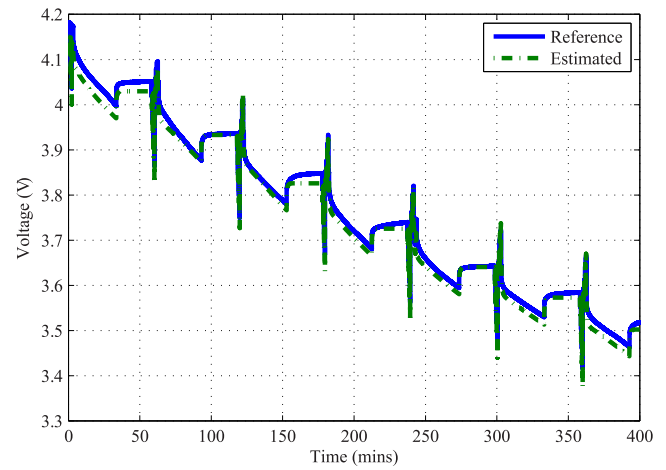

Fig. 7.   Comparison of experimental and estimated voltages of discharge pulses.
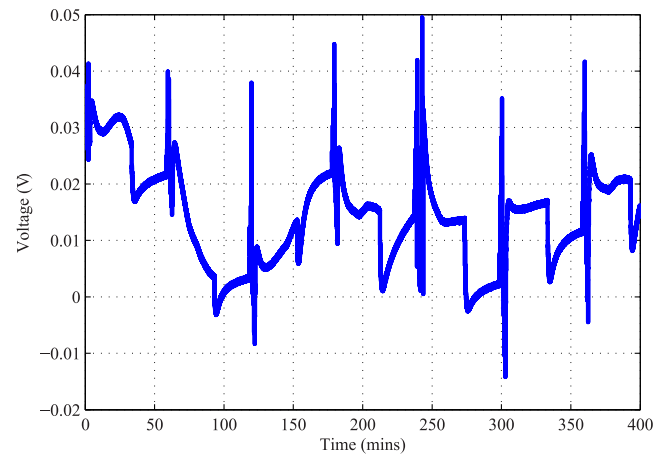

Fig. 8.   Voltage estimation error of discharge pulses.

From Fig. 8, the results show that the state space model of the battery using the identified battery parameters could accurately estimate the battery voltage. The mean estimation error is 10 mV and the maximum error is 50 mV at the time that the charge and discharge pulses are applied.

III. SQUARE ROOT SPHERICAL UNSCENTED KALMAN FILTER (SQRT-UKFST) BASED SOC ESTIMATION

The EKF has been extensively used in the SOC estimation in the literatures [5], [11], [21], [33]. Although the EKF performs well by integrating with other estimation methods including observers and neural network; it experiences limitation such as the filter stability due to Jacobian matrices [34]. To achieve better stability and accuracy, the UKF has been introduced as it does not require the computation of Jacobian matrices. The UKF uses a selection of weighted sigma points to estimate the sample mean and covariance. In the following sections, the unit hyper sphere spherical unscented transform and the Sqrt-UKFST algorithms are presented.

TABLE II
PROPOSED UNIT HYPER SPHERE SPHERICAL UNSCENTED TRANSFORM

Step 1: Choose the initial weight, W_0
$$0 \le W_0 \le 1$$
Step 2: Compute the rest of the weights, W_i
$$W_i = \frac{1 - W_0}{n + 1}$$
Step 3: Initialize the following element vectors
$$\chi_0^1 = [0], \chi_1^1 = \left[-\frac{1}{\sqrt{2W_1}} \right], \chi_2^1 = \left[\frac{1}{\sqrt{2W_1}} \right]$$
Step 4: Recursively expand the following vectors, for $j = 2, \ldots, n,$
$$\chi_i^j = \begin{cases} \begin{bmatrix} \chi_0^{j-1} \\ 0 \end{bmatrix} & \text{for } i = 0 \\[8pt] \begin{bmatrix} \chi_1^{j-1} \\ -\frac{1}{\sqrt{j(j+1)W_1}} \end{bmatrix} & \text{for } i = 1, \ldots, j \\[8pt] \begin{bmatrix} 0_{j-1} \\ \frac{j}{\sqrt{j(j+1)W_1}} \end{bmatrix} & \text{for } i = j+1 \end{cases}$$
Step 5: Arrange χ_i^j vectors in a unit hyper sphere
$$\frac{\chi_i^j}{\sqrt{n}/(1 - W_0)}$$

A. Unit Hyper Sphere Spherical Unscented Transform

There are several sigma point transformation methods: unscented, simplex, and spherical transforms. Due to the fact that the computation cost of UKF is proportional to the number of sigma points, it is beneficial to have fewer sigma points. The unscented transform requires $2n+1$ sigma points selection, where n is dimension of the system. The simplex transform requires only $n+1$ sigma points. However, it suffers from numerical stability issues due to the fact that the sigma points lie on the sphere with a radius of $2^{n/2}$ [35].

The spherical transform considered in this paper for SOC estimation requires $n+2$ sigma points. However, its numerical stability is improved by reducing the sphere radius to $\sqrt{n}/(1 - W_0)$. In the spherical transform of an n dimensional system, the initial weight W_0 is set first and the choice of W_0 affects only the fourth- and higher-order moments of the set of sigma points. Using W_0 and n, the rest of the weight (W_1 to W_n) are selected. The three element vectors (χ_0^1, χ_1^1, and χ_2^1) are generated using W_1. To generate the required $n+2$ set of sigma point vectors with n dimension, the element vectors are recursively expanded.

In this study, it was discovered that several stability issues remain in the spherical transform UKF, such as negative battery parameters. This is due to the fact that the sphere radius for sigma point distribution depends on the size of estimated state vector. To ensure the sphere radius is independent on the estimated state vector size, and ζ always falls within the range of the expected variance of $f(\zeta)$, all sigma points are normalized with respect to $\sqrt{n}/(1 - W_0)$. Thus, all the sigma points are guaranteed to be projected within a unit hyper sphere. The spherical transform is summarized in Table II.

B. Square Root Unscented Kalman Filter

In a standard UKF, the state covariance P_k is recursively updated and propagated by decomposing into matrix square root, S_k, for sigma point mapping at each time step where $P_k = S_k S_k^T$. Then, P_k matrix is reconstructed from all the propagated sigma points for updating purpose. On the other hand,

TABLE III
SPHERICAL SQUARE ROOT UNSCENTED KALMAN FILTER

Step1: Set the initial state mean $\hat{x}_0 = \begin{bmatrix} \zeta & V_D & V_K \end{bmatrix}^T$ and covariance S_0:
$$\hat{x}_0 = E[x_0], S_0 = chol\{E[(x_0 - \hat{x}_0)(x_0 - \hat{x}_0)^T]\}$$
Step 2: Compute the sigma points χ_i,
$$\chi_{i,k-1} = \hat{x}_{k-1} + S_{k-1}\chi_i^n, i = 0, 1, \ldots, n+1$$
where χ_i^j is computed based on *Step1–5* in Table II
Step 3: State estimates propagation
$$\chi_{k|k-1} = F(\chi_{k-1}, u_{k-1})$$
Step 4: Calculation of mean estimates,
$$\hat{x}_k^- = \begin{bmatrix} \hat{\zeta}_k^- & \hat{V}_D^- & \hat{V}_K^- \end{bmatrix}^T = \sum_{i=0}^{n+1} W_i \chi_{k|k-1}$$
where W_i is computed in **Step 2** in Table II
Step 5: Square root covariance propagation and update,
$$S_k^- = qr\{[\sqrt{W_i}(\chi_{1:n+1,k|k-1} - \hat{x}_k^-)\sqrt{Q}]\}$$
$$S_k^- = cholupdate\{S_k^-, \chi_{0,k|k-1} - \hat{x}_k^-, W_0\}$$
Step 6: Calculation of estimated measurement Υ_k and mean $\hat{y}_k^-$
$$\Upsilon_{k|k-1} = H[\chi_{k|k-1}]\hat{y}_t^- = \hat{V}_t^- = \sum_{i=0}^{n+1} W_i \Upsilon_{i,k|k-1}$$
Step 7: Compute the measurement covariance $S_{\tilde{y}_k}$ and its update
$$S_{\tilde{y}_k} = qr\{[\sqrt{W_i}(\Upsilon_{1:n+1,k|k-1} - \hat{y}_k^-)\sqrt{R}]\}$$
$$S_{\tilde{y}_k} = cholupdate\{S_{\tilde{y}_k}, \Upsilon_{0,k|k-1} - \hat{y}_k^-, W_0\}$$
Step 8: Calculation of cross covariance matrix $P_{x_k y_k}$
$$P_{x_k y_k} = \sum_{i=0}^{n+1} W_i(x_{i,k|k-1}^+ - \hat{x}_k^-)(\Upsilon_{i,k|k-1} - \hat{y}_k^-)^T$$
Step 9: Calculation of Kalman gain K_k and state estimate update $\hat{x}_k^+$ through measurement ($y_k = V_t$)
$$K_k = P_{x_k y_k} S_{\tilde{y}_k}^{T^{-1}} S_{\tilde{y}_k}^{-1}$$
$$\hat{x}_k^+ = \hat{x}_k^- + K_k(y_k - \hat{y}_k^-)$$
Step 10: Covariance matrix update
$$U = K_k S_{\tilde{y}_k}$$
$$S_k = cholupdate\{S_k^-, U, -1\}$$

First, the initial covariance and state estimates are selected. Then, *Steps 2* to *10* are recursively processed until end of the experiment (or input data).

the Sqrt-UKFST directly propagates and updates the S_k without the needs of decomposing and reconstructing matrix P_k. This avoids the needs of refactorization on P_k at each time step. Thus positive semidefiniteness of the P_k could be guaranteed [22]. The square root UKF makes use of three linear algebra techniques for square-root covariance update and propagation: QR decomposition (*qr*), Cholesky factor updating (*cholupdate*) and efficient least squares [22].

Given an n dimensional state space model of a nonlinear system and output equations as follows:

$$x_{k+1} = f(x_k, u_k) + Q_k \tag{9}$$

$$y_k = h(x_k, u_k) + R_k \tag{10}$$

where u_k is the system input variables, x_k is the system state variables and y_k is the state output variables. The state-space and the measurement models are *f(x,u)* and *h(x,u)* respectively. Let $Q_k - N(0, \text{cov}_Q)$ and $R_k - N(0, \text{cov}_R)$ represent the Gaussian process and measurement noises respectively. Through the spherical transform, the n state variables can be transformed into $n+2$ sigma points χ_i with the weight w_i (see Table II). The sigma points are propagated through the state function $f(x_k, u_k)$ in (9). These propagated sigma points are used to estimate the system output, *y,* using $h(x_k, u_k)$ in (6). The Kalman filter gain K is calculated through S_k and the cross covariance P_{xy}. Then the state mean and covariance are updated using the computed
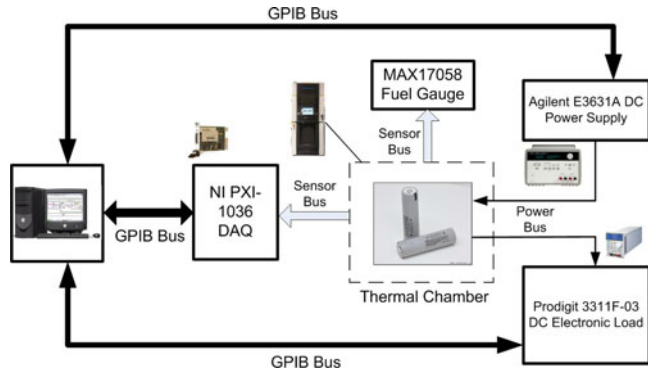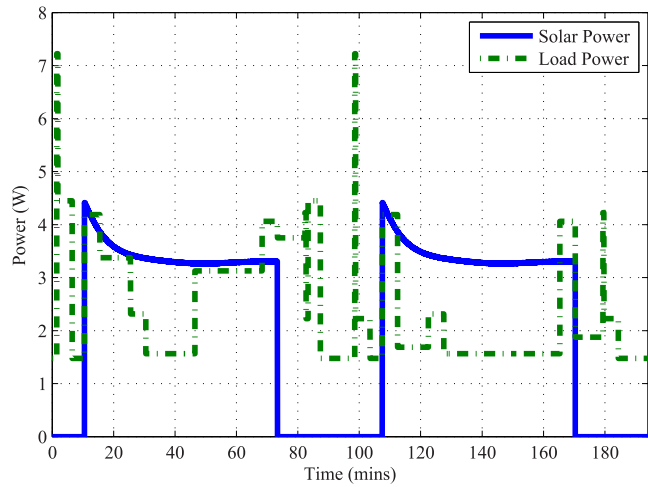
Fig. 9. Experimental setup.

Fig. 10. LEO satellite solar power and load profiles.

Fig. 11. SOC estimation with unknown initial state.

Fig. 12. SOC estimation error under unknown initial SOC.

Kalman gain, K. Table III summarizes the Sqrt-UKFST algorithm.

IV. EXPERIMENTAL RESULTS AND DISCUSSION

To validate the proposed method, a battery test bench has been set up as shown in Fig. 9. The setup is used to perform a satellite mission scenario of a low earth orbit (LEO) profile. Fig. 10 shows the orbit profile used in the experiment with an orbital period of 97 min.

As shown in Fig. 9, a dc power supply (Agilent E3631A) is used to simulate the output solar power and a dc Electronic Load (Prodigit 3311F-03) is used to simulate the loadings of satellite subsystems. A data acquisition system (NI PXI-1036) is used to record the battery terminal voltage, terminal current and temperature for reference SOC calculation. The reference SOC is obtained using the calibrated ampere hour counting via the high precision current sensors from the power supply and the dc electronic load with the sensor accuracy of 0.2% and 0.1% respectively. A LabVIEW program has been written to control all the hardware equipment. A thermal chamber (SE-300) is used to maintain the battery temperature at 25 °C to emulate the battery heater in maintaining the satellite battery temperature. A microcontroller (100MHz C8051F120) is used
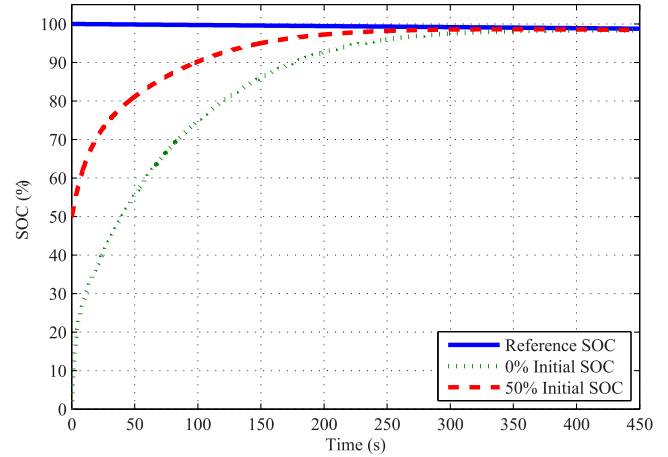
to process the acquired data as well as the real-time experimental SOC for comparison. In addition, a portable fuel gauge (MAX17058) with an expected accuracy of 3–5% is used for further benchmarking.

A. SOC Estimation With Unknown Initial State

First, the performance of SOC estimation using the proposed Sqrt-UKFST with unknown initial SOC is performed. The true SOC is set as 100% and the two initial estimated SOC are 0% and 50%. Fig. 11 shows that the estimated SOC converges to the true SOC within 250 s when the initial estimated SOC error is assumed to be 50%. With the initial SOC error sets to 100%, the proposed method is able to converge to the true SOC after 300 s. To further validate the convergence performance of the proposed method, Fig. 12 summarizes the SOC estimation errors after 300 s of different initial estimated SOC for four different reference SOC. The four reference SOC are 30%, 50%, 75%, and 100%. From Fig. 12, the Sqrt-UKFST is able to converge to the reference SOC across the entire operation range with the maximum estimation error of 2.4%. The results show that the
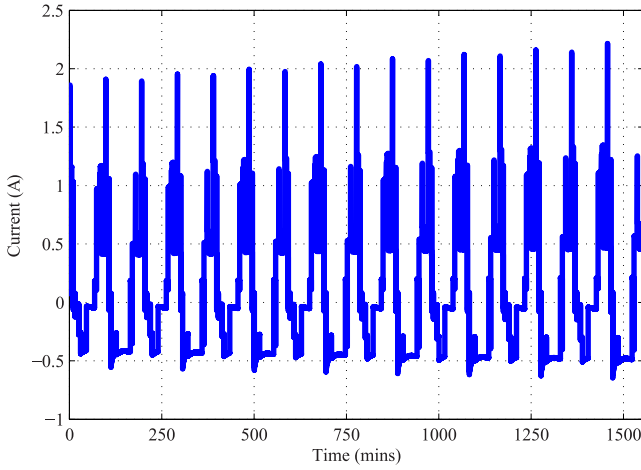
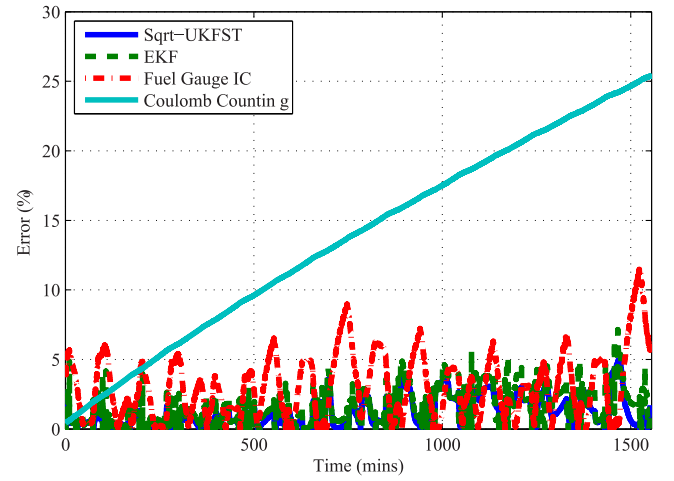Fig. 13.   Battery current profile under orbital test experiment.

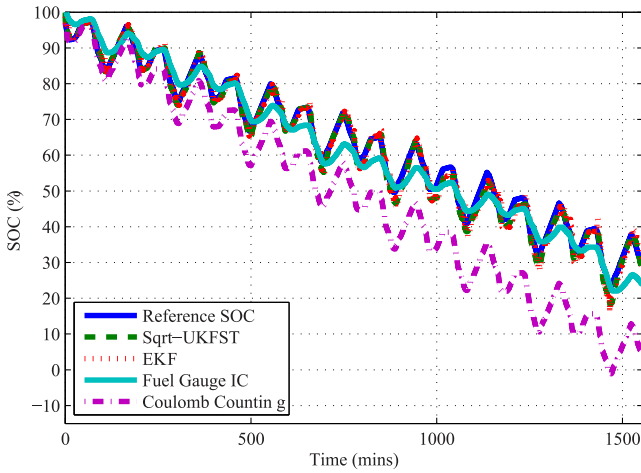Fig. 15.   SOC estimation error comparison.

Fig. 14.   SOC estimation comparison.

TABLE IV
PERFORMANCE COMPARISON

		Sqrt-UKFST	EKF	Fuel gauge	Coulomb counting
RMSE	Absolute value	1.42%	1.95%	3.85%	15.48%
	% increase w.r.t SqrtUKFST	-	37.32%	171.13%	990%
Mean error	Absolute value	1.09%	1.54%	3.09%	13.73%
	% increase w.r.t Sqrt-UKFST	-	41.28%	183%	1153%
Maximum error	Absolute value	4.96%	7.15%	11.47%	25.38%
	% increase w.r.t Sqrt-UKFST	-	44.15%	131.30%	411.69%

initial estimation error does not impact the convergence of the SOC estimation using the proposed Sqrt-UKFST.

B. SOC Estimation With Known Initial State

The initial state of SOC is known whenever the battery is fully charged. Fig. 13 shows the experimental results of battery current with 16 satellite orbits using the load profile in Fig. 10. In this experiment, the battery is fully charged before the test is commenced.

Fig. 14 shows the corresponding SOC estimation using various approaches. From the results, it is observed that the SOC based on the Coulomb counting method drifted away from the reference SOC due to the accumulated errors. Moreover, it is noticed that both EKF and Sqrt-UKFST perform better than the fuel gauge.

To evaluate the performance of different SOC estimation methods, the absolute mean, maximum and root mean square

errors (RMSE) of the SOC are calculated as follows:

$$\text{Mean} = \frac{1}{n} \sum_{k=1}^{n} \left| \zeta_k - \hat{\zeta}_k \right|$$
$$\text{RMSE} = \sqrt{\frac{1}{n} \sum_{k=1}^{n} \left(\zeta_k - \hat{\zeta}_k \right)^2} \qquad (11)$$
$$\text{Maximum} = \text{Max} \left| \zeta_k - \hat{\zeta}_k \right|.$$

The percentage SOC estimation error is plotted in Fig. 15. From the results, it is observed that the Coulomb counting error increases linearly due to the accumulated errors. For the fuel gauge circuit, its SOC estimation relies solely on the voltage readings. Since the battery voltage increases when it is being charged and vice versa, the fuel gauge circuit experiences higher fluctuations in SOC estimation than EKF and Sqrt-UKFST whenever a charge/discharge current is applied. Both EKF and Sqrt-UKFST have similar SOC estimation error.

Table IV summarizes the results. It shows that the Sqrt-UKFST has the lowest RMSE of 1.42%, absolute mean error of 1.19%, and maximum error of 4.96%. For the EKF, its errors are about 40% higher than Sqrt-UKFST. Furthermore, the fuel

TABLE V
MULTIPLICATION REQUIRED FOR EACH OPERATION

	Multiplication required		
Operation	Spherical unscented transform	Unscented transform	EKF
P_{xx}	$(n+2)n^2$	$(2n+1)n^2$	-
P_{xy}	$(n+2)(nL)$	$(2n+1)(nL)$	-
P_{yy}	$(n+2)L^2$	$(2n+1)L^2$	-
$PH^T(HPH^T+R)$	-	-	$L^3+2nL^2+2n^2L$
$K(y-\hat{y})$	L^3+nL^2+nL	L^3+nL^2+nL	$nL+Ln^2$
$P-KP_{yy}K$	Ln^2	Ln^2	n^2L+n^3
Total multiplication required ($n = 3$, $L = 1$)	81	107	73

TABLE VI
DIFFERENT PARAMETERS SETS USED IN SENSITIVITY ANALYSIS

	R_0 (mΩ)	R_D (mΩ)	R_K (mΩ)	C_D (F)	C_K (F)
True parameters (p)	54.28	10.58	40.16	330	1020
Group 1 (0.25p)	13.57	2.65	10.04	82.5	255
Group 2 (0.5p)	27.14	5.29	20.08	165	510
Group 3 (0.75p)	40.71	7.94	30.12	247.5	765
Group 4 (1.25p)	67.85	13.23	50.2	412.5	1275
Group 5 (1.5p)	81.42	15.87	60.24	495	1530
Group 6 (1.75p)	94.99	18.52	70.28	577.5	1785
Group 7 (2p)	108.56	21.06	80.32	660	2040

gauge estimation error is at least 100% higher than the Sqrt-UKFST. It is noted that the Coulomb counting mean error is almost ten times higher than the Sqrt-UKFST.

C. Computational Requirements

Table V compares the number of multiplication required in each operation for the spherical unscented transform, regular unscented transform, and EKF. In the table, "*n*" denotes the number of states and "*L*" is the number of measurements. From the table, it is observed that the spherical unscented transform requires less multiplication than the regular unscented transform as a result of using fewer sigma points. For the SOC estimation ($n = 3$ and $L = 1$), the total number of multiplication is 81 for the spherical unscented transform and 107 for the unscented transform. Thus there is a 32% saving in multiplication using the proposed approach.

D. Robustness of SOC Estimation With Battery's Parameters Variation

The accuracy of SOC estimation is affected by the battery model accuracy. The battery parameters may vary depending on the battery's SOH [36]. As the battery usage increases, its parameters such as R_O would change. The variation could be as high as 60% of initial parameters [37]. To study the robustness of the proposed approach and EKF with respect to parameters variation, different battery parameter sets are used. Table VI presents different sets of parameters in terms of 25%, 50%, 75%, 125%, 150%, 175%, and 200% of the actual battery parameters.
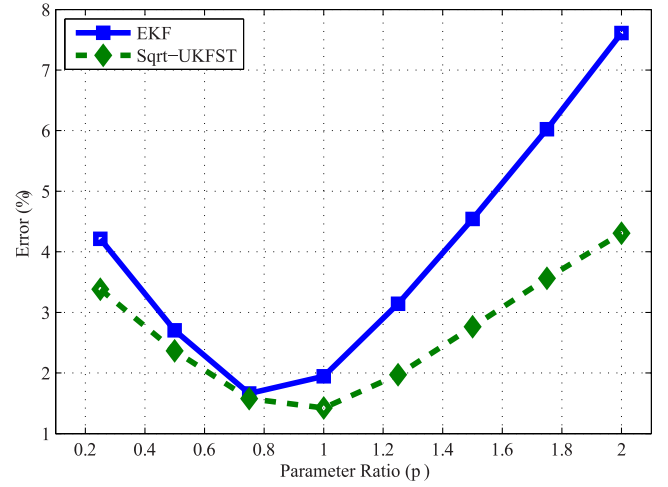

Fig. 16. RMSE comparison with different parameters set between EKF and Sqrt-UKFST.
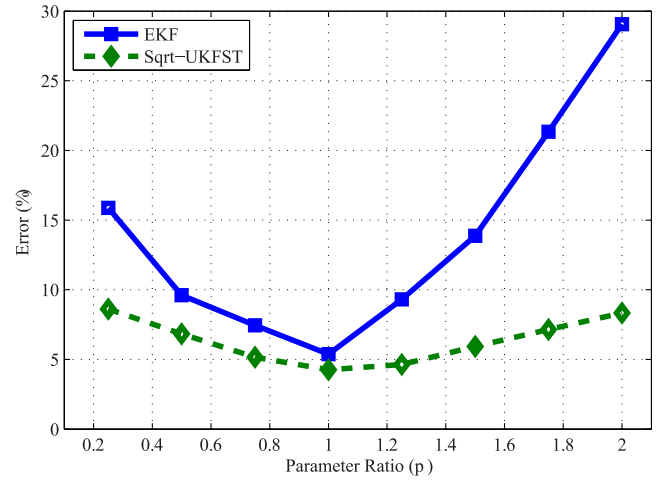

Fig. 17. Absolute maximum SOC error comparison with different parameters set between EKF and Sqrt-UKFST.

For groups 1 to 3, the true battery parameters are higher than the estimated parameters, and groups 4 to 7 provide the case that the true parameters are lower than the estimated parameters.

The parameters in each group are used by Sqrt-UKFST and EKF to estimate the SOC. Figs. 16 and 17 show the RMSE and absolute maximum error. Both figures show that Sqrt-UKFST has lower error than EKF. Fig. 16 shows that the highest RMSE for EKF and Sqrt-UKFST are 7.6% and 4.3% respectively. The absolute maximum error for EKF can be as high as 29% while Sqrt-UKFST remains below 8%. In summary, the Sqrt-UKFST is more robust to parameter variation than EKF.

V. CONCLUSION

Using the double polarization lithium-ion battery model, a new SOC estimation method using Sqrt-UKFST is presented. The proposed method takes advantage of Jacobian-free linearization approach with UKF. The spherical transform with hyper unit sphere requires fewer sigma points than the standard

UKF and provides a better controllability of the sigma point distribution. In addition, the square root characteristic of the proposed approach improves the numerical properties in state covariance. The experimental results of the proposed approach have been compared with EKF, Coulomb counting, and fuel gauge. The RMSE results have shown that EKF, Coulomb counting, and fuel gauge are approximately 37%, 900%, and 171% higher than the proposed method respectively. In addition, the parameter variation study shows that the proposed Sqrt-UKFST is more robust than EKF. Furthermore, computational analysis shows that regular UKF requires 32% more multiplication than Sqrt-UKFST.

REFERENCES

[1] K. Rajashekara, "Present status and future trends in electric vehicle propulsion technologies," *IEEE J. Emerg. Sel. Topics Power Electron.*, vol. 1, pp. 3–10, Apr. 2013.

[2] M. Yilmaz and P. T. Krein, "Review of battery charger topologies, charging power levels, and infrastructure for plug-in electric and hybrid vehicles," *IEEE Trans. Power Electron.*, vol. 28, pp. 2151–2169, May 2013.

[3] W. Waag, C. Fleischer, and D. U. Sauer, "Critical review of the methods for monitoring of lithium-ion batteries in electric and hybrid vehicles," *J. Power Sources*, vol. 258, pp. 321–339, Mar. 2014.

[4] J. C. A. Anton, P. J. G. Nieto, F. J. d. C. Juez, F. S. Lasheras, C. B. Viejo, and N. R. Gutierrez, "Battery state-of-charge estimator using the MARS technique," *IEEE Trans. Power Electron.*, vol. 28, pp. 3798–3805, Aug. 2013.

[5] J. Kim, S. Lee, and B. H. Cho, "Complementary cooperation algorithm based on DEKF combined with pattern recognition for SOC/capacity estimation and SOH prediction," *IEEE Trans. Power Electron.*, vol. 27, pp. 436–451, Jan. 2012.

[6] M. Gholizadeh and F. R. Salmasi, "Estimation of state of charge, unknown nonlinearities, and state of health of a lithium-ion battery based on a comprehensive unobservable model," *IEEE Trans. Ind. Electron.*, vol. 61, pp. 1335–1344, Mar. 2014.

[7] R. Xiong, H. He, F. Sun, and K. Zhao, "Evaluation on state of charge estimation of batteries with adaptive extended Kalman filter by experiment approach," *IEEE Trans. Veh. Technol.*, vol. 62, pp. 108–117, Jan. 2013.

[8] A. H. Ranjbar, A. Banaei, A. Khoobroo, and B. Fahimi, "Online estimation of state of charge in Li-ion batteries using impulse response concept," *IEEE Trans. Smart Grid*, vol. 3, pp. 360–367, Mar. 2012.

[9] Z. Chen, Y. Fu, and C. C. Mi, "State of charge estimation of lithium-ion batteries in electric drive vehicles using extended Kalman filtering," *IEEE Trans. Veh. Technol.*, vol. 62, pp. 1020–1030, Mar. 2013.

[10] M. Coleman, C. K. Lee, C. Zhu, and W. G. Hurley, "State-of-charge determination from EMF voltage estimation: Using impedance, terminal voltage, and current for lead-acid and lithium-ion batteries," *IEEE Trans. Ind. Electron.*, vol. 54, pp. 2550–2557, Oct. 2007.

[11] M. Charkhgard and M. Farrokhi, "State-of-charge estimation for lithium-ion batteries using neural networks and EKF," *IEEE Trans. Ind. Electron.*, vol. 57, pp. 4178–4187, Dec. 2010.

[12] I. H. Li, W. Wei-Yen, S. Shun-Feng, and L. Yuang-Shung, "A merged fuzzy neural network and its applications in battery state-of-charge estimation," *IEEE Trans. Energy Convers.*, vol. 22, pp. 697–708, Sep. 2007.

[13] J. Kim, J. Shin, C. Chun, and B. H. Cho, "Stable configuration of a Li-ion series battery pack based on a screening process for improved voltage/SOC balancing," *IEEE Trans. Power Electron.*, vol. 27, pp. 411–424, Jan. 2012.

[14] D. Jie, J. Seuss, L. Suneja, and R. G. Harley, "SoC feedback control for wind and ESS hybrid power system frequency regulation," *IEEE J. Emerg. Sel. Topic Circuits Syst.*, vol. 2, pp. 79–86, Mar. 2014.

[15] K. S. Ng, C.-S. Moo, Y.-P. Chen, and Y.-C. Hsieh, "Enhanced coulomb counting method for estimating state-of-charge and state-of-health of lithium-ion batteries," *Appl. Energy*, vol. 86, pp. 1506–1511, Sep. 2009.

[16] A. A. H. Hussein and I. Batarseh, "A review of charging algorithms for nickel and lithium battery chargers," *IEEE Trans. Veh. Technol.*, vol. 60, pp. 830–838, Mar. 2011.

[17] J. C. A. Anton, P. J. G. Nieto, C. B. Viejo, and J. A. V. Vilan, "Support vector machines used to estimate the battery state of charge," *IEEE Trans. Power Electron.*, vol. 28, pp. 5919–5926, Dec. 2013.

[18] F. Zhang, G. Liu, L. Fang, and H. Wang, "Estimation of battery state of charge with H∞ observer: Applied to a robot for inspecting power transmission lines," *IEEE Trans. Ind. Electron.*, vol. 59, pp. 1086–1095, Feb. 2012.

[19] I. L.-S. Kim, "A technique for estimating the state of health of lithium batteries through a dual-sliding-mode observer," *IEEE Trans. Power Electron.*, vol. 25, pp. 1013–1022, Apr. 2010.

[20] I. S. Kim, "Nonlinear state of charge estimator for hybrid electric vehicle battery," *IEEE Trans. Power Electron.*, vol. 23, pp. 2027–2034, Jul. 2008.

[21] J. Kim and B. H. Cho, "State-of-charge estimation and state-of-health prediction of a Li-ion degraded battery based on an EKF combined with a per-unit system," *IEEE Trans. Veh. Technol.*, vol. 60, pp. 4249–4260, Nov. 2011.

[22] S. S. Haykin, *Kalman Filtering and Neural Networks*. New York, NY, USA: Wiley, 2001.

[23] H. Gholizade-Narm and M. Charkhgard, "Lithium-ion battery state of charge estimation based on square-root unscented Kalman filter," *Power Electronics, IET*, vol. 6, pp. 1833–1841, Nov. 2013.

[24] Z. He, M. Gao, C. Wang, L. Wang, and Y. Liu, "Adaptive state of charge estimation for Li-ion batteries based on an unscented Kalman filter with an enhanced battery model," *Energies*, vol. 6, pp. 4134–4151, Aug. 2013.

[25] W. He, N. Williard, C. Chen, and M. Pecht, "State of charge estimation for electric vehicle batteries using unscented Kalman filtering," *Microelectron. Rel.*, vol. 53, pp. 840–847, Jan. 2013.

[26] M. Partovibakhsh and G. Liu, "Online estimation of model parameters and state-of-charge of lithium-ion battery using unscented Kalman filter," in *Proc. Am. Control Conf.*, Jun. 2012, pp. 3962–3967.

[27] W. Wang, H. S.-H. Chung, and J. Zhang, "Near-real-time parameter estimation of an electrical battery model with multiple time constants and SOC-dependent capacitance," *IEEE Trans. Power Electron.*, vol. 29, pp. 5905–5920, Nov. 2014.

[28] L. Gao, S. Liu, and R. A. Dougal, "Dynamic lithium-ion battery model for system simulation," *IEEE Trans. Compon. Packag. Technol.*, vol. 25, pp. 495–505, Sep. 2002.

[29] M. Chen and G. A. Rincon-Mora, "Accurate electrical battery model capable of predicting runtime and I-V performance," *IEEE Trans. Energy Convers.*, vol. 21, pp. 504–511, Jun. 2006.

[30] C. Zheng and K. S. Low, "A virtual instrument for the testing and performance evaluation of a microsatellite power supply system," *IEEE Trans. Instrum. Meas.*, vol. 57, pp. 1808–1815, Aug. 2008.

[31] H. Aung and K. S. Low, "Modeling and state of charge estimation of a lithium ion battery using unscented Kalman filter in a nanosatellite," in *Proc. 9th IEEE Conf. Ind. Electron. Appl.*, Jun. 2014.

[32] M. Einhorn, F. V. Conte, C. Kral, and J. Fleig, "Comparison, selection, and parameterization of electrical battery models for automotive applications," *IEEE Trans. Power Electron.*, vol. 28, pp. 1429–1437, Mar. 2013.

[33] H. He, R. Xiong, X. Zhang, F. Sun, and J. Fan, "State-of-charge estimation of the lithium-ion battery using an adaptive extended Kalman filter based on an improved Thevenin model," *IEEE Trans. Veh. Technol.*, vol. 60, pp. 1461–1469, May 2011.

[34] J. L. Crassidis and J. L. Junkins, *Optimal Estimation of Dynamic Systems*, 2nd ed. Boca Raton, FL: CRC Press, 2012.

[35] S. J. Julier, "The spherical simplex unscented transformation," in *Proc. Am. Control Conf.*, vol. 3, Jun. 2003, pp. 2430–2434.

[36] L. Long and P. Bauer, "Practical capacity fading model for Li-ion battery cells in electric vehicles," *IEEE Trans. Power Electron.*, vol. 28, pp. 5910–5918, Dec. 2013.

[37] D. Haifeng, W. Xuezhe, and S. Zechang, "A new SOH prediction concept for the power lithium-ion battery used on HEVs," in *Proc. IEEE Veh. Power Propulsion Conf.*, Sep. 2009, pp. 1649–1653.

Htet Aung (S'12) received the B.Eng. degree in electrical and electronic engineering (electrical and system engineering) from Nanayang Technological University, Singapore, in 2011, where he is currently working toward the Ph.D. degree.

His main research interests include battery modeling, parameters identification, state-of-charge, state-of-health estimation, and satellite power subsystems.

Kay-Soon Low (M'88–SM'00) received the B.Eng. degree from the National University of Singapore, Singapore, in 1985, and the Ph.D. degree from the University of New South Wales, Sydney, Australia, in 1994, both in electrical engineering.

He was with the academia as well as the industry. He joined the School of Electrical and Electronic Engineering, Nanyang Technological University, in 1994 first as a Lecturer and subsequently became an Associate Professor. He has successfully supervised 42 graduate theses and delivered 43 funded projects. He has served as consultants to many companies and has 19 patents on nonlinear circuits, UWB systems, and imaging sensor. His funded projects are in the field of wireless sensor network, power electronics, solar energy, and satellite system. Since April 2009 he has been the Centre Director of Satellite Research Centre (SaRC), Nanyang Technological University. The centre has successfully developed four satellites (X-SAT, VELOX-PII, VELOX-PIII, and VELOX-I) and they have been launched between April 2011 and June 2014. In orbit experiments such as fault tolerant power management system, peak power tracker for solar energy, and model predictive control of satellite attitude have been successfully demonstrated.

Shu Ting Goh received the Ph.D. degree from the Mechanical Engineering—Engineering Mechanics Department, Michigan Technological University, in 2012.

He is currently a Research Fellow in Satellite Research Centre, School of Electrical and Electronic Engineering, Nanyang Technological University. His research interests include the parameter optimization, data assimilation, attitude determination, and Kalman filter implementation on photovoltaic module characteristic identification, battery state of charge estimation, acoustic tracking and localization, satellite attitude and position estimation, and object tracking.